Planetary boundary layer and atmospheric turbulence.

Szymon P. Malinowski
Marta Wacławczyk

Institute of Geophysics UW

2017/18

Lecture 12

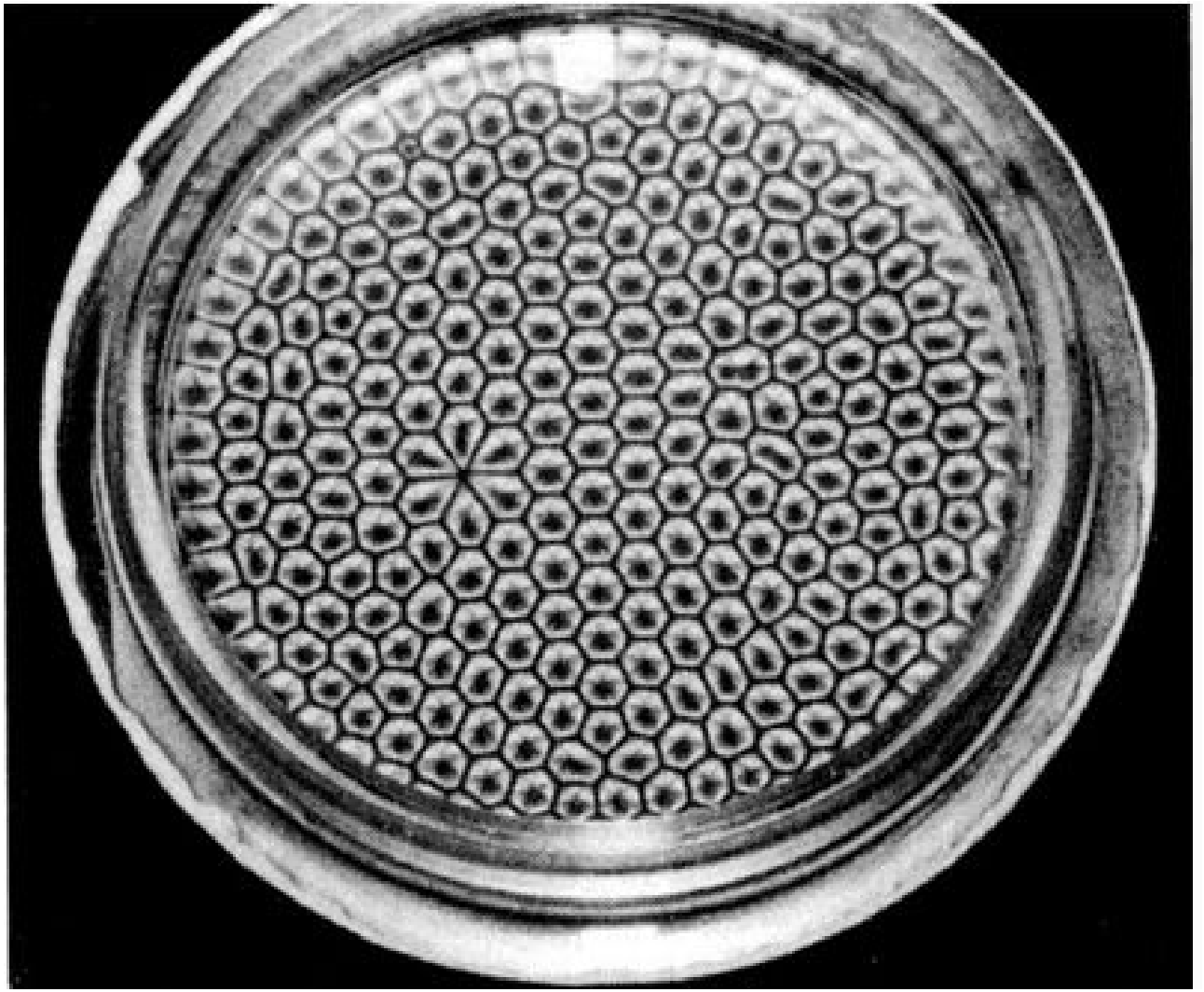

Rayleigh – Benard convection

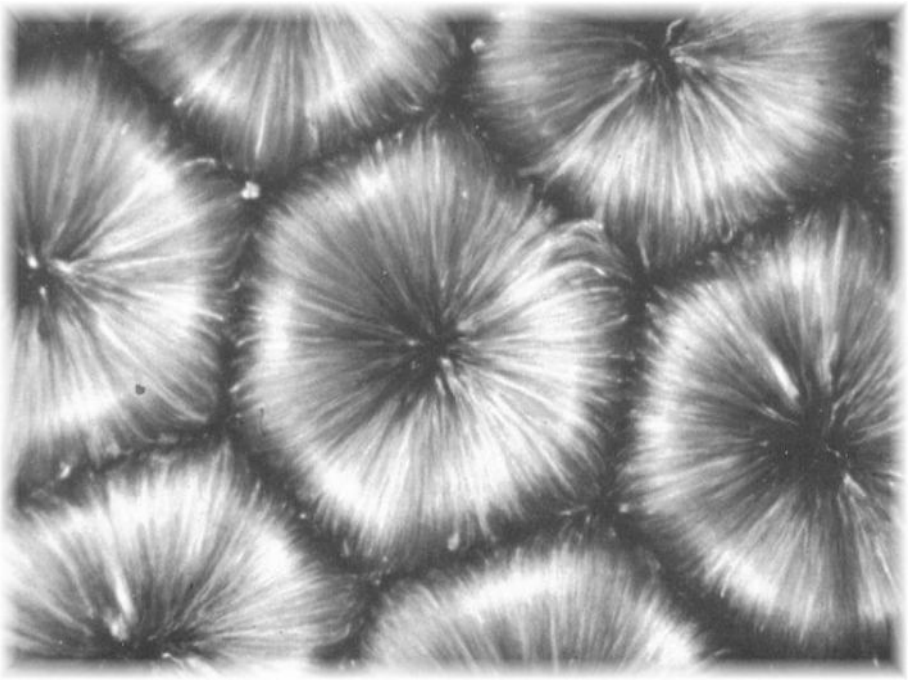

Laboratory

R-B convection by molecular dynamics

Solar chromosphere

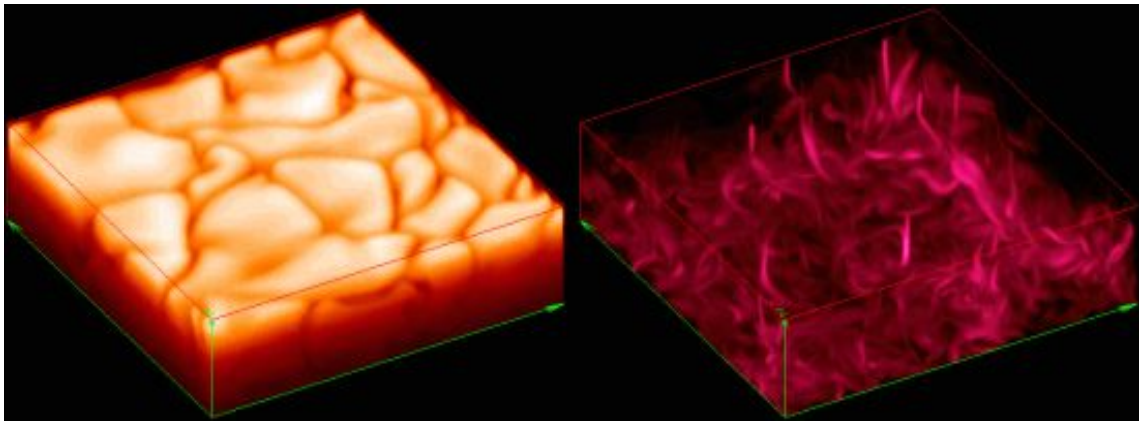

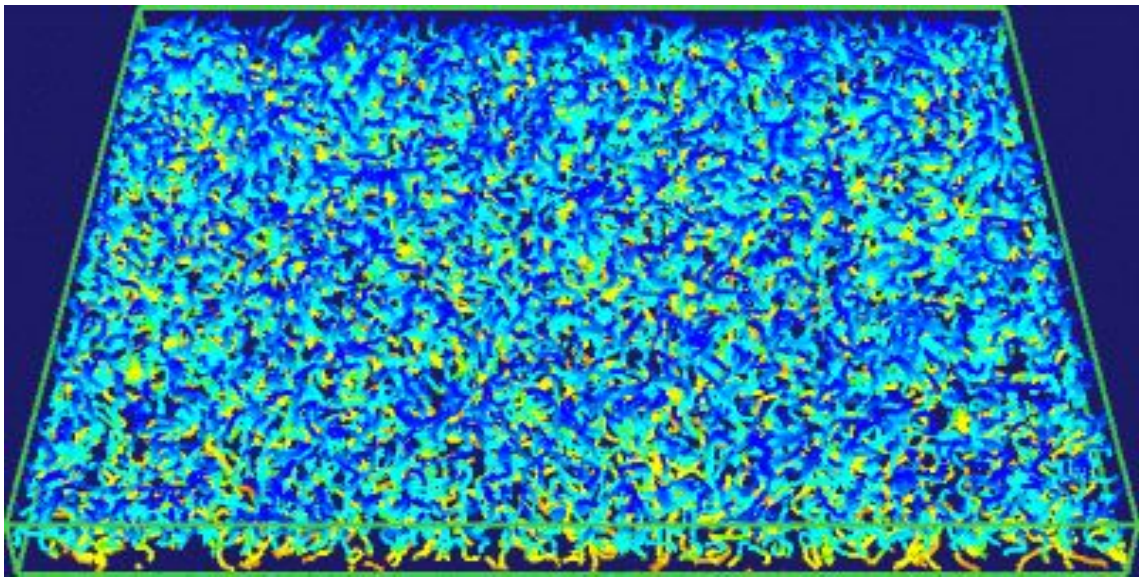

H. Bénard. Les tourbillons cellulaires dans une nappe liquide. *Rev. Gen. Sci. Pures Appl.*, 11:1261–1271, 1900.

L. Rayleigh. On convection currents in a horizontal layer of fluid, when the higher temperature is on the under side. *Philos. Mag.*, 32:529–546, 1916.

Motivation:

Simulations with realistic topography with 1km grid resolution feed by boundary conditions from the operational NWP mesoscale model show characteristic patterns of open cells (updrafts in BL marked with red) and formation of clouds (blue) above.

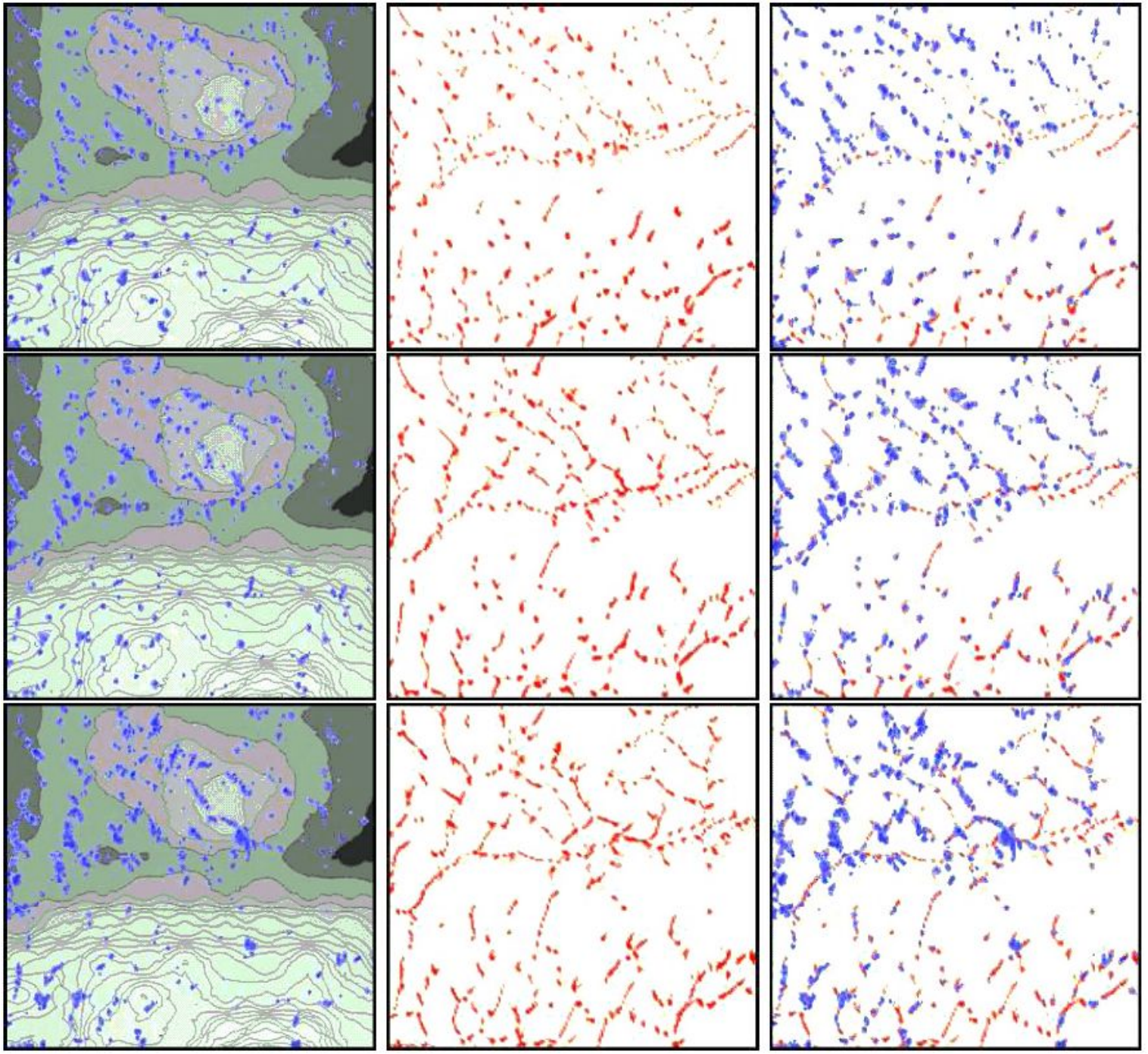

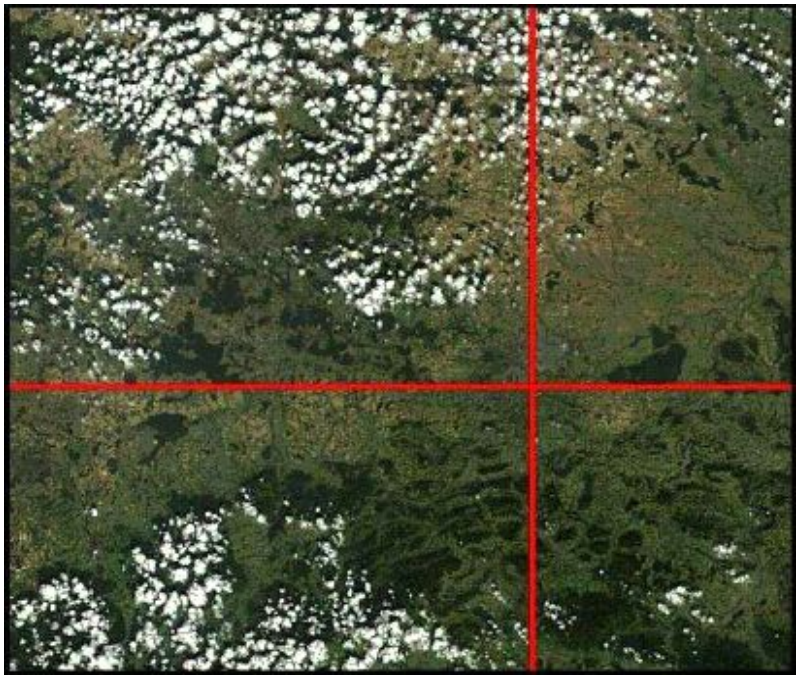

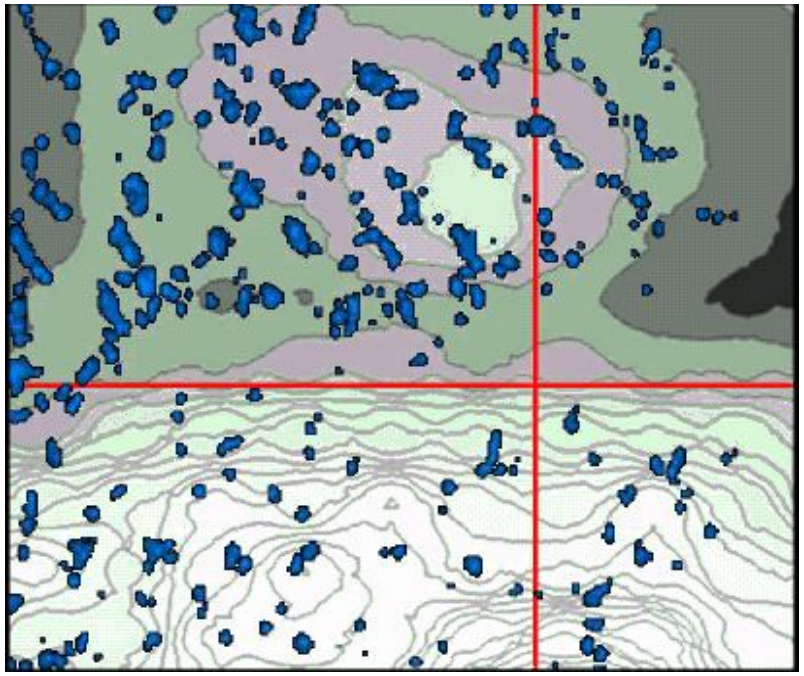

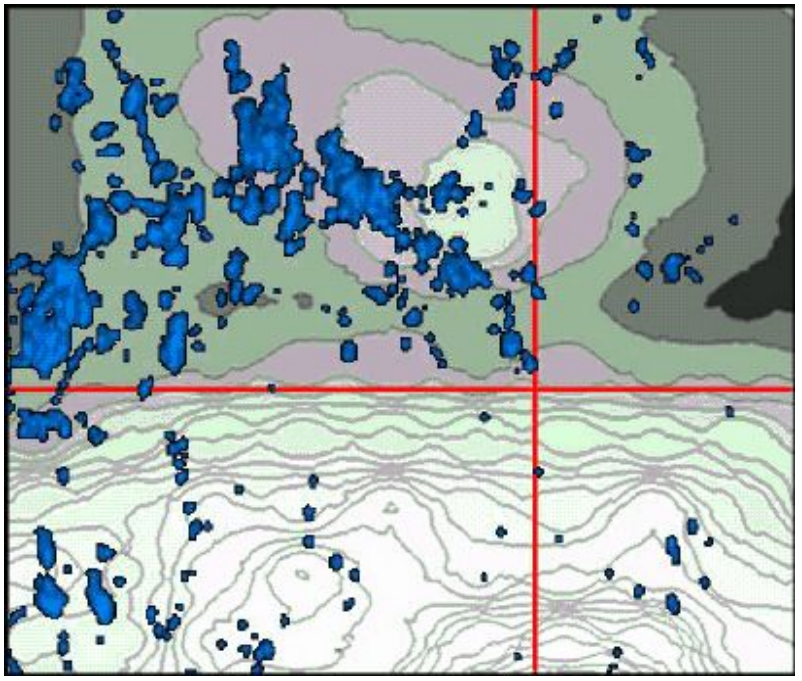

09:45 local time

11:30 local time

2004.09.07

Comparison of EULAG simulations to satellite images show qualitative agreement in terms of regions with cloud development and unrealistic cloud patterns.

Rayleigh number: $$Ra = \frac{g\Delta\overline{\theta}h^3}{\overline{\theta}\nu\nu_\theta}$$

rigid – stress-free boundary

Ra_c=1100.657

In the atmosphere:

h= 1000 m

ν = 1.7 x 10^-5

ν_θ =1.9 x 10^-5

Δθ /θ = 0.1 x 10^-2

→ **Ra=10^16 !!!**

So how could we get cellular convection at all?

Modified definition (Jeffreys, 1928):

$$Rz = \frac{g\Delta\overline{\theta}h^3}{\overline{\theta}K_m^2}$$

K_m - effective „eddy diffusivity”

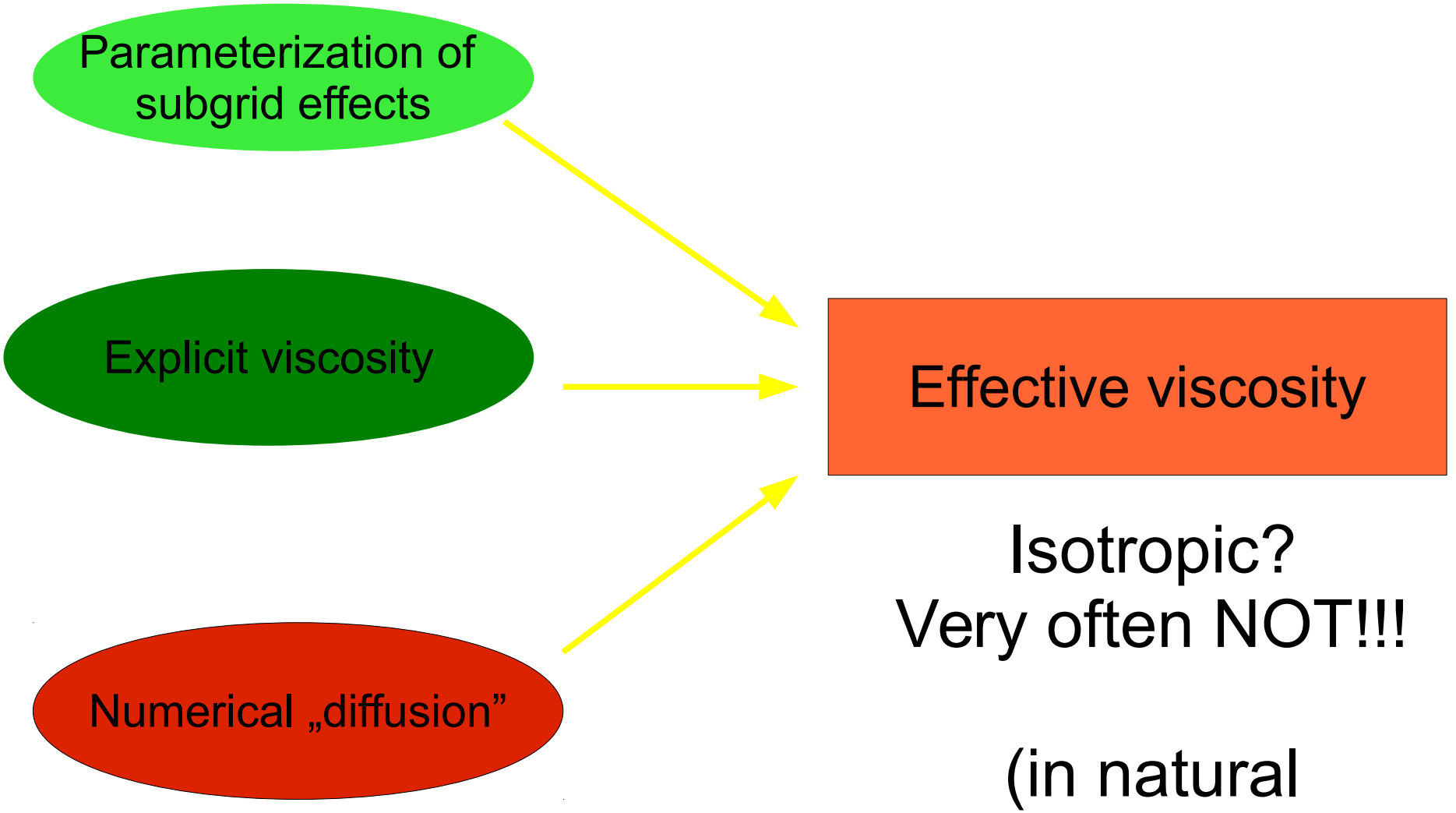

Isotropic?
Very often NOT!!!

(in natural atmospheric flows Prestley, 1962)

Vertical velocities after 6h of simulated time are shown within the PBL depth. Grey iso-surfaces represent clouds, and dark green patterns mark updrafts at boundary layer top. Isolines and other colors show the topography.

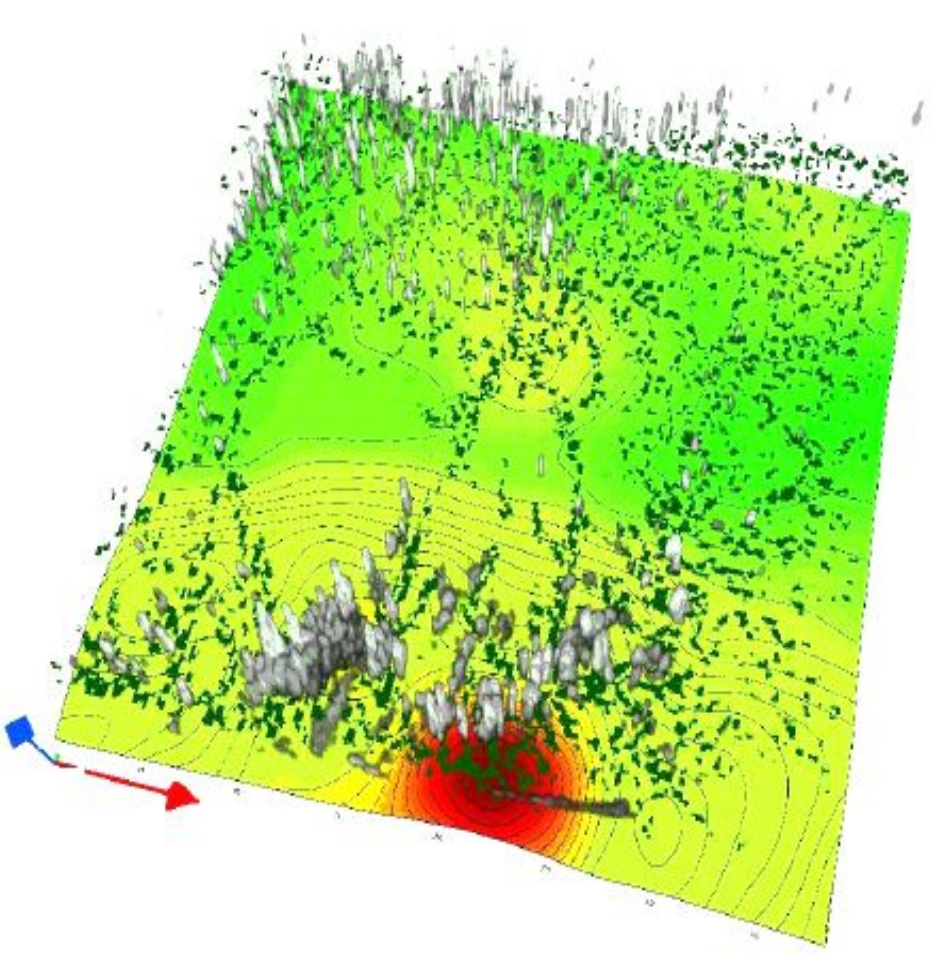

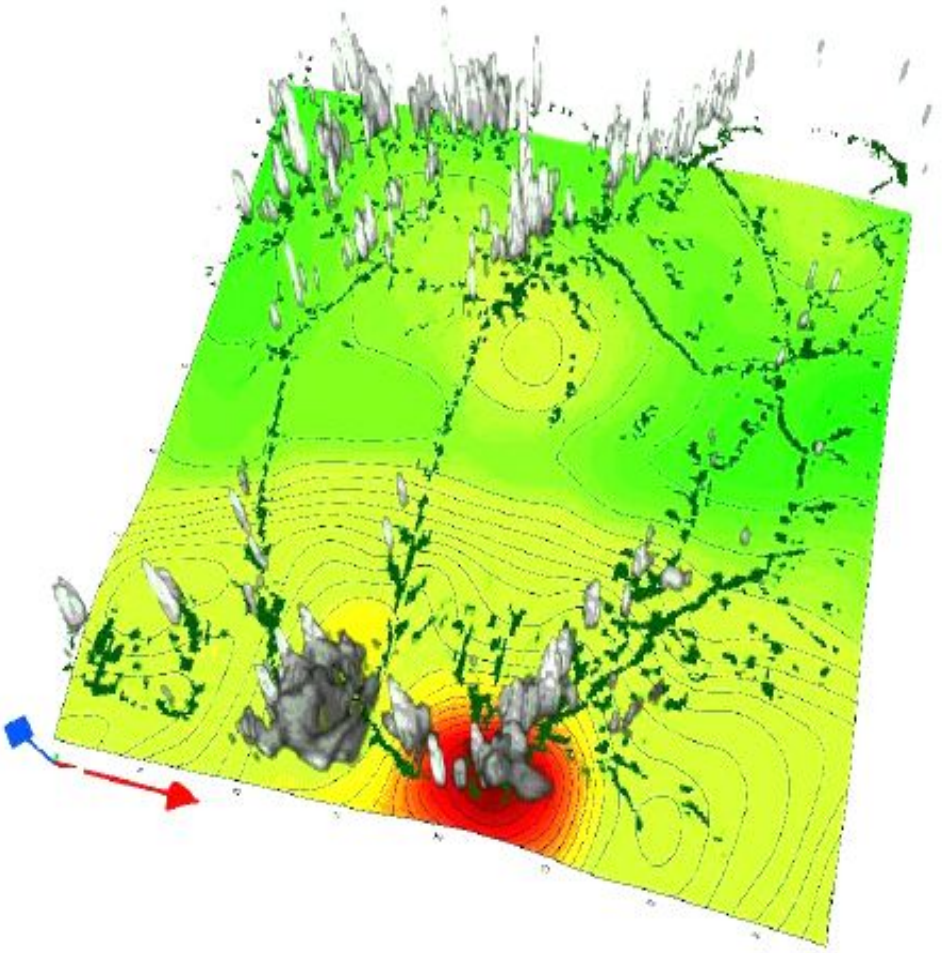

Sensitivity studies show clear dependence of simulated cloud patterns and updrafts within BPL on the the effective viscosity of numerical advection.

Long history of investigating atmospheric cellular convection

[1] L. Rayleigh, On convection currents in a horizontal layer of fluid, when the higher temperature is on the under side, Phil. Mag 32 (6) (1916) 529–546.

[2] C. Priestley, Width-height ratio of large convection cells, Tellus 14 (1962) 123–124.

[3] D. Ray, Cellular convection with nonisotropic eddys., Tellus 17 (1965) 434–439.

[4] P. Sheu, E. Agee, J. Tribbia, A numerical study of physical processes affecting convective cellular geometry, J. Meteor. Soc. Japan, 58 (1980) 489–499.

[5] B. Atkinson, J. Zhang, Mesoscale shallow convection in the atmosphere, Rev. Geophys. 34 (1996) 403–431.

.. however, the problem is unclarified yet, and new elements are introduced when performing numerical approximation.

Linear theory

We assume the incompressible Boussinesq system linearized around a static reference state, allow for different dissipative/diffusive forcings in the horizontal and the vertical

$$\frac{\partial \mathbf{u}}{\partial t} = -\nabla \phi + g\alpha\theta\nabla z + \nu_h \Delta_h \mathbf{u} + \nu_v \Delta_z \mathbf{u},$$
$$\frac{\partial \theta}{\partial t} = \beta w + \kappa_h \Delta_h \theta + \kappa_v \Delta_z \theta,$$
$$\nabla \cdot \mathbf{u} = 0.$$

u is the velocity vector with w denoting vertical component; φ is the normalized pressure perturbation; g and α are, respectively, the acceleration of gravity and the coefficient of the volume expansion; θ is potential temperature deviation from a linear profile with adverse gradient β; and subscripts h and v refer to the horizontal and vertical, respectively.

After mathematical manipulations we end with the marginal stability criterion:

$$Ra_h(k,r) = \frac{H^4}{k^2}\left(n^2\left(\frac{\pi}{\frac{H}{\sqrt{r}}}\right)^2 + k^2\right)^3 \frac{\left(n^2\left(\frac{\pi}{H}\right)^2 + k^2\right)}{\left(n^2\left(\frac{\pi}{H}\right)^2 r + k^2\right)},$$

where $r=\nu_v/\nu_h=\kappa_v/\kappa_h$, H is depth and k is a wavenumber.

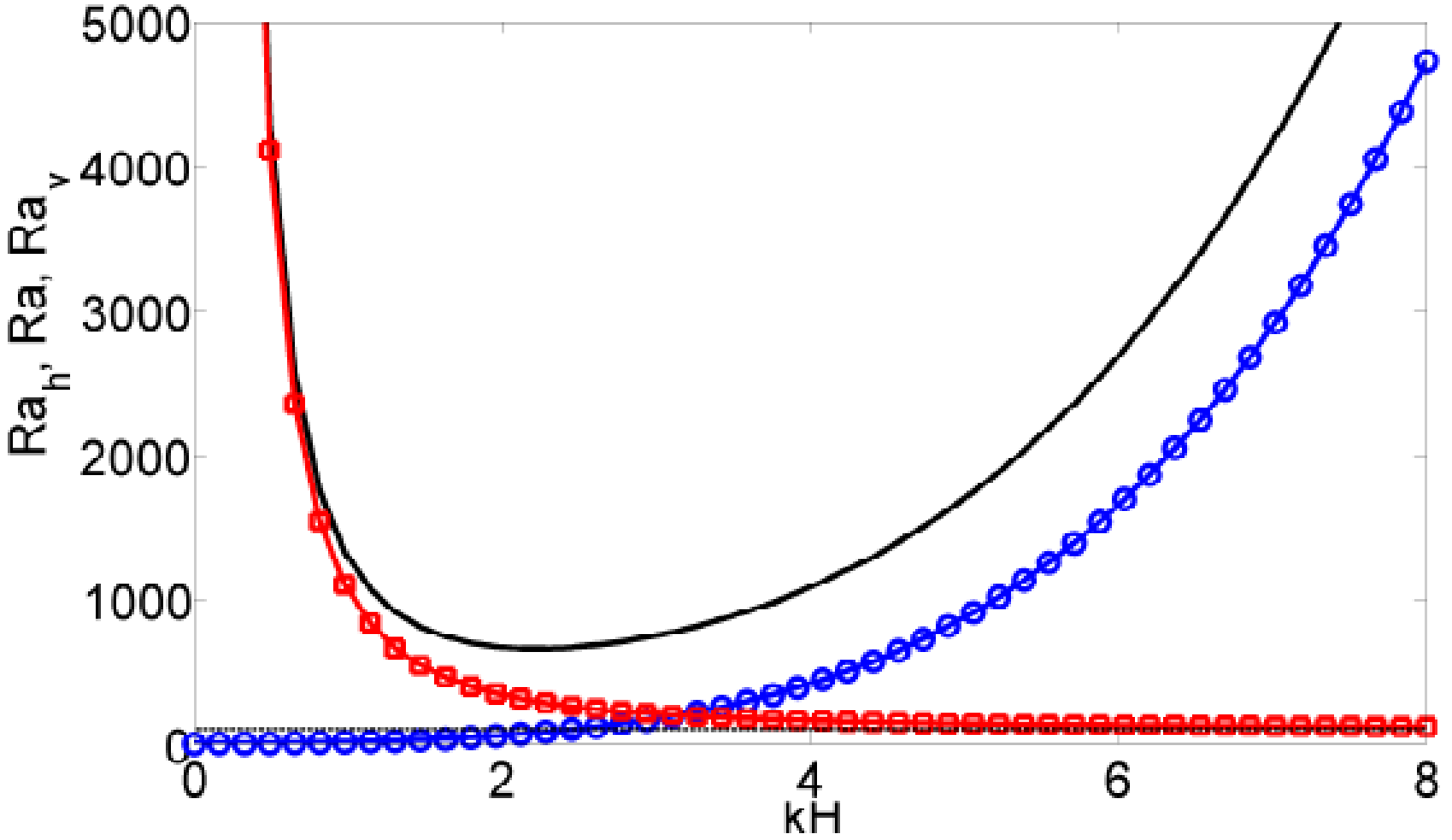

FIGURE 2.2.1. Asymptotic marginal stability relations for $\nu_h = \nu_v$ (solid), $\nu_v = 0$ (circles) and $\nu_h = 0$ (squares) at a finite Prandtl number. Respective Rayleigh numbers Ra_h, Ra and Ra_v are shown as functions of the squared horizontal wave number (2.2.5). For each curve the stability region lies beneath.

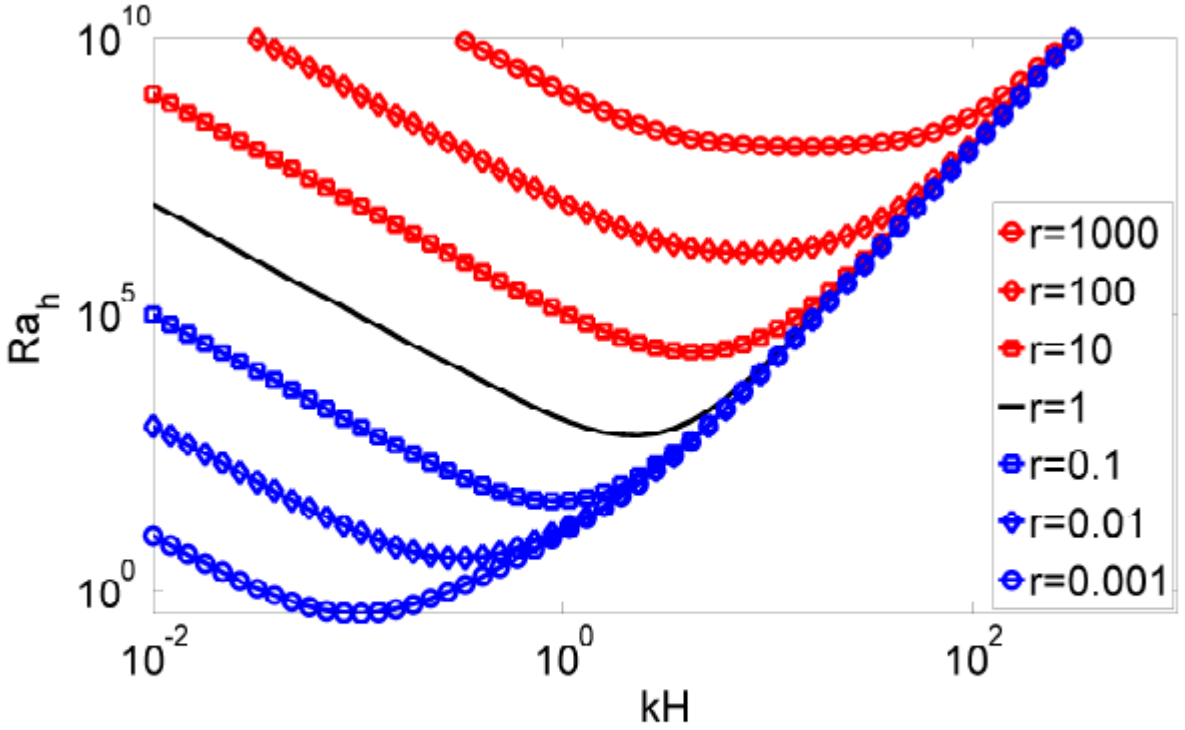

FIGURE 2.2.2. Marginal stability relation (2.2.14) for finite anisotropy ratios $r = 10^{-3}, .., 10^{3}$.

Figure 2.2.2 illustrates (2.2.14) for a range of disperse values of the anisotropy ratio r at $n = 1$. It conveys that at a fixed value of Ra_h, the range of unstable horizontal modes diminishes with increasing anisotropy ratio r. Furthermore, Fig. 2.2.2 shows that as the anisotropy ratio increases, the critical Rayleigh number Ra_h increases monotonically; whereas the wavelength of the marginally stable mode diminishes gradually. The converse can be concluded for the analysis in terms of

Numerical verification

LES simulations with dry Boussinesq mode of EULAG model:

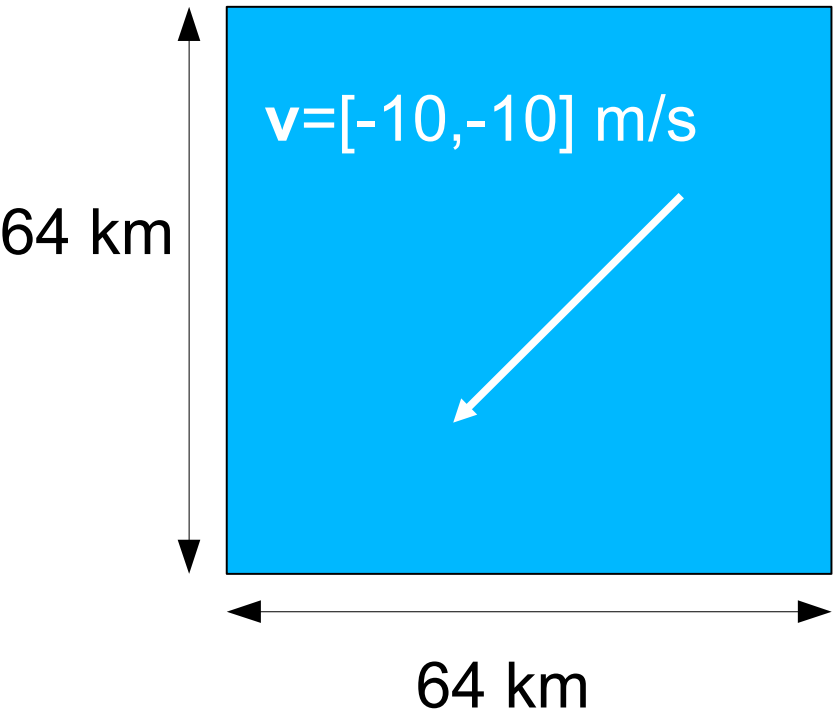

dz=50 m

dx=dy≈500 m

Heat flux
hfx=200 W/m^2

Flat terrain

Cylic horizontal boundary condition

Reference setup – resembling modern mesoscale cloud resolving Numerical Weather Prediciton

Simplified simulations – no mean wind

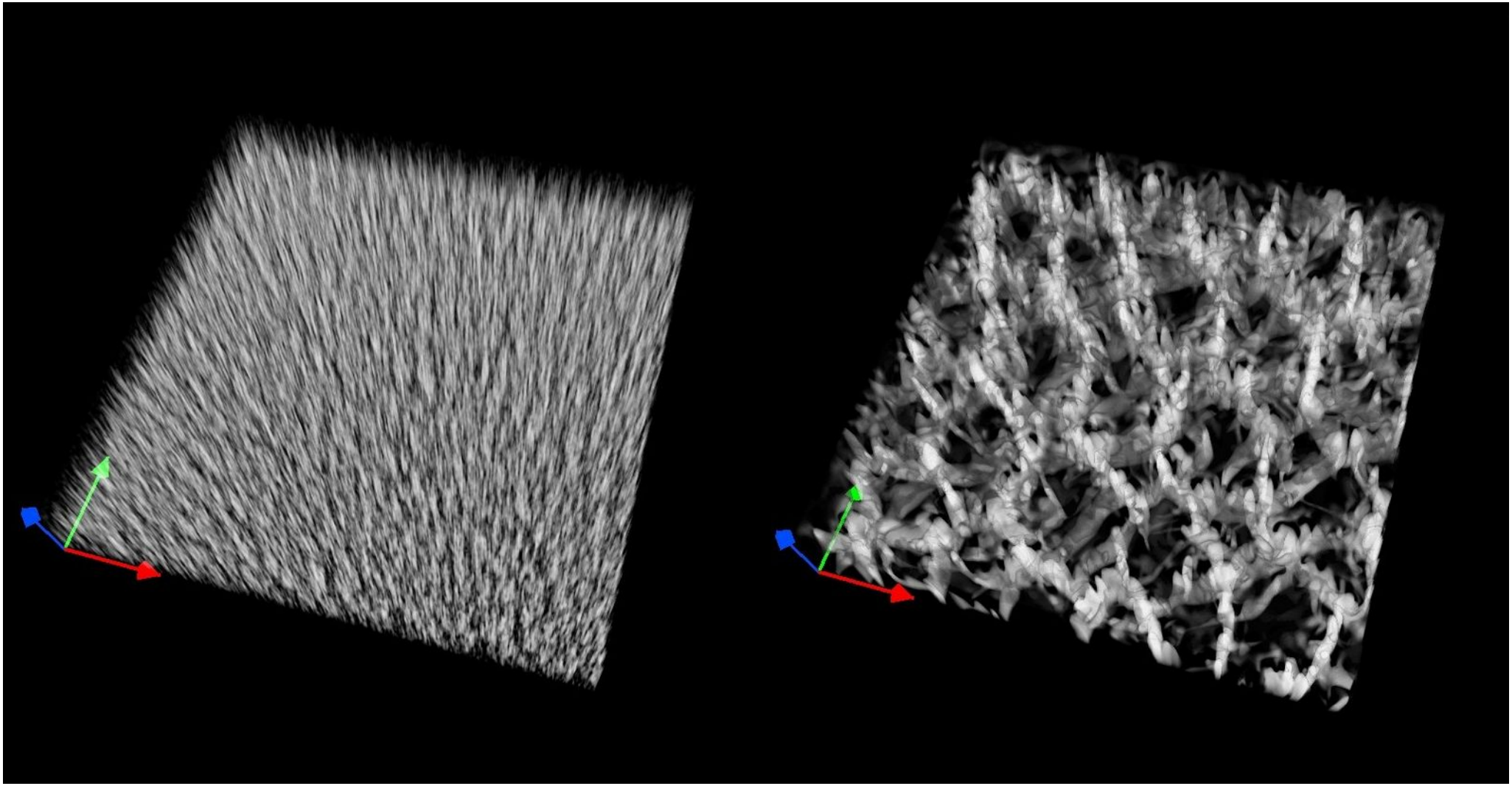

Structure of thermal convection over heated plate. Vertical velocities after 6h of simulated time are shown within the PBL depth. Bright and dark volumes denote updrafts and downdrafts, respectively. The only difference between the two solutions is the value of viscosity in horizontal entries of the stress tensor, $v_h = 2.5$ *and* $v_h = 70\ m^2 s^{-1}$ *, while constant vertical entry is* $v_v = 2.5\ m^2 s^{-1}$

Sources of diffusivity in numerical simulations:

- - diffusive numerical methods (e.g. UPWIND)
- - composite schemes (e.g. UPWIND every 4^{th} step
- - different numerical schemes in horizontal and in vertical

  - diffusive filters
-
-
- Tests: hundred of simulations, various approaches, grid sizes and resolutions.....

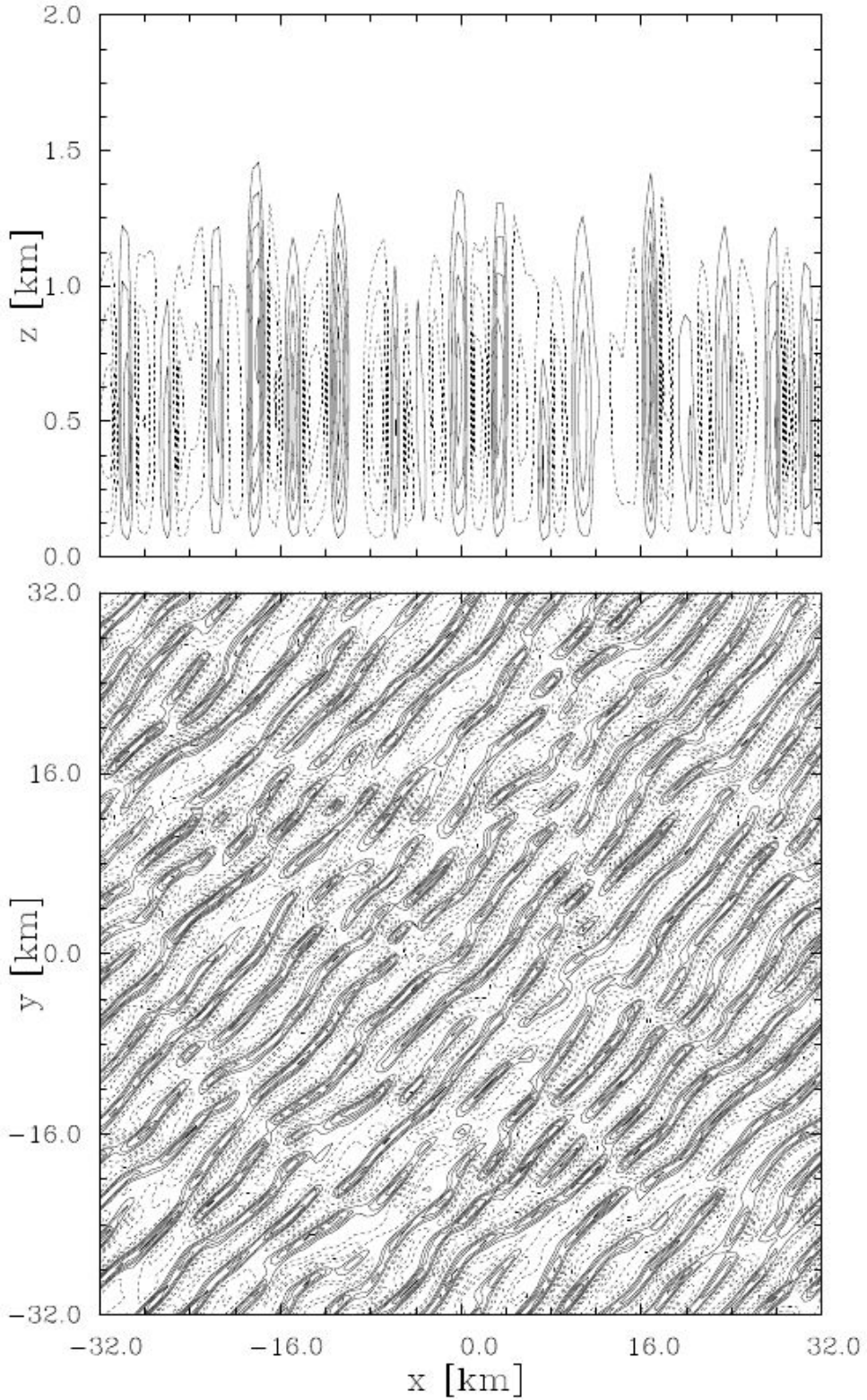

FIGURE 4.2.3. Reference simulation: contours of vertical velocity in central xz plane (top) and in the xy plane at $z = 450$ m (bottom) at $t = 4$ h of the simulated time. The contour interval is 0.5 ms^{-1} in both panels; solid/dashed lines are for positive/negative field values, and zero contour lines are not shown.

Example 1:

what horizontal grid spacing to resolve convective roll width ?

60 m !

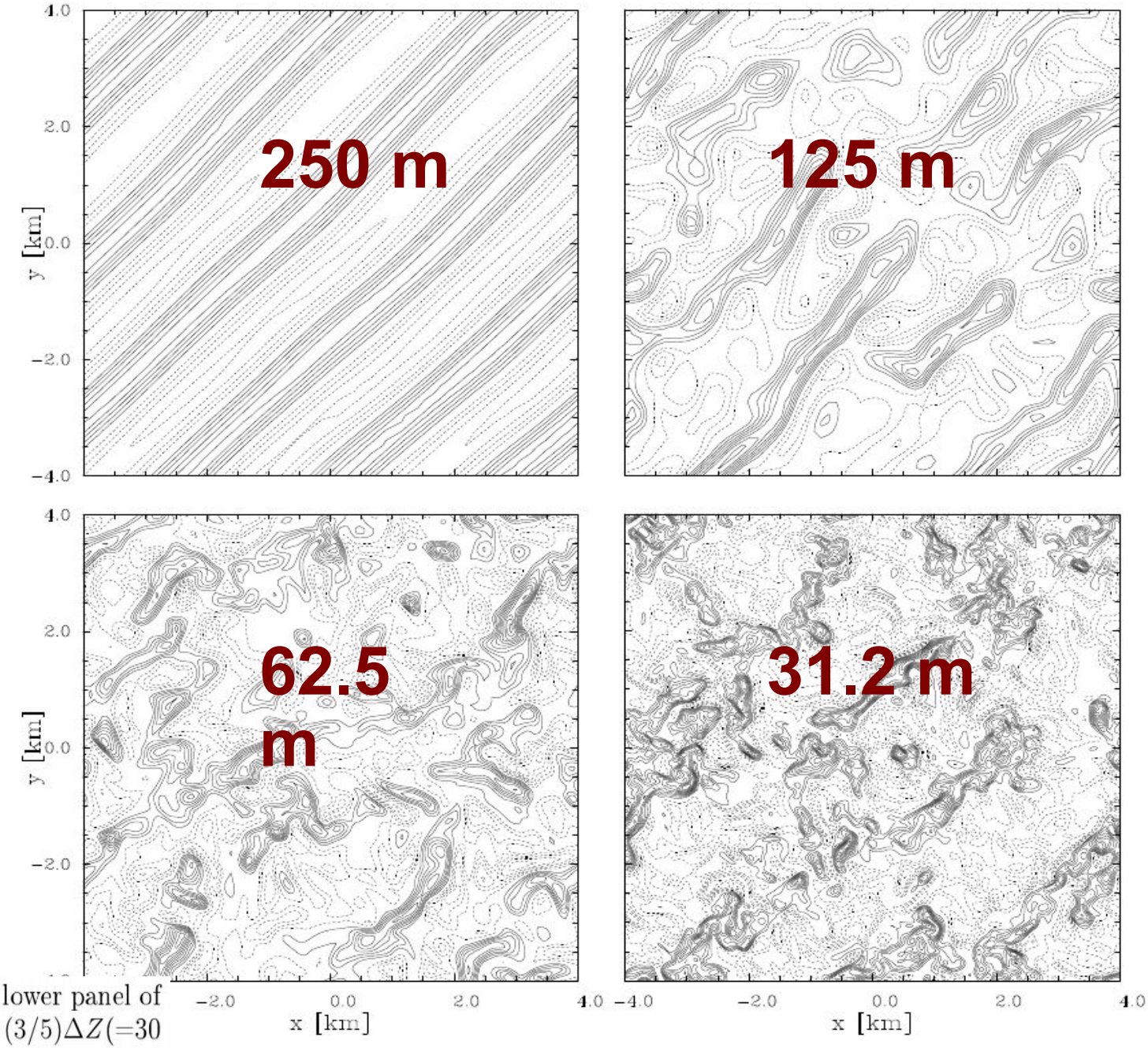

FIGURE 4.3.1. Vertical velocity as in the lower panel of Fig. 4.2.3, using finer vertical resolution $(3/5)\Delta Z$(=30 m) and smaller 8×8 km horizontal domain resolved with $32^2(\Delta_H = 250$ m), $64^2(\Delta_H = 125$ m), $128^2(\Delta_H = 62.5$ m) and $256^2(\Delta_H = 31.25$ m) grid points in the upper left, upper right, lower left, and lower right panel, respectively.

Example 2:

what horizontal domain size to get two rolls resolved ?

> 4 x 4km !

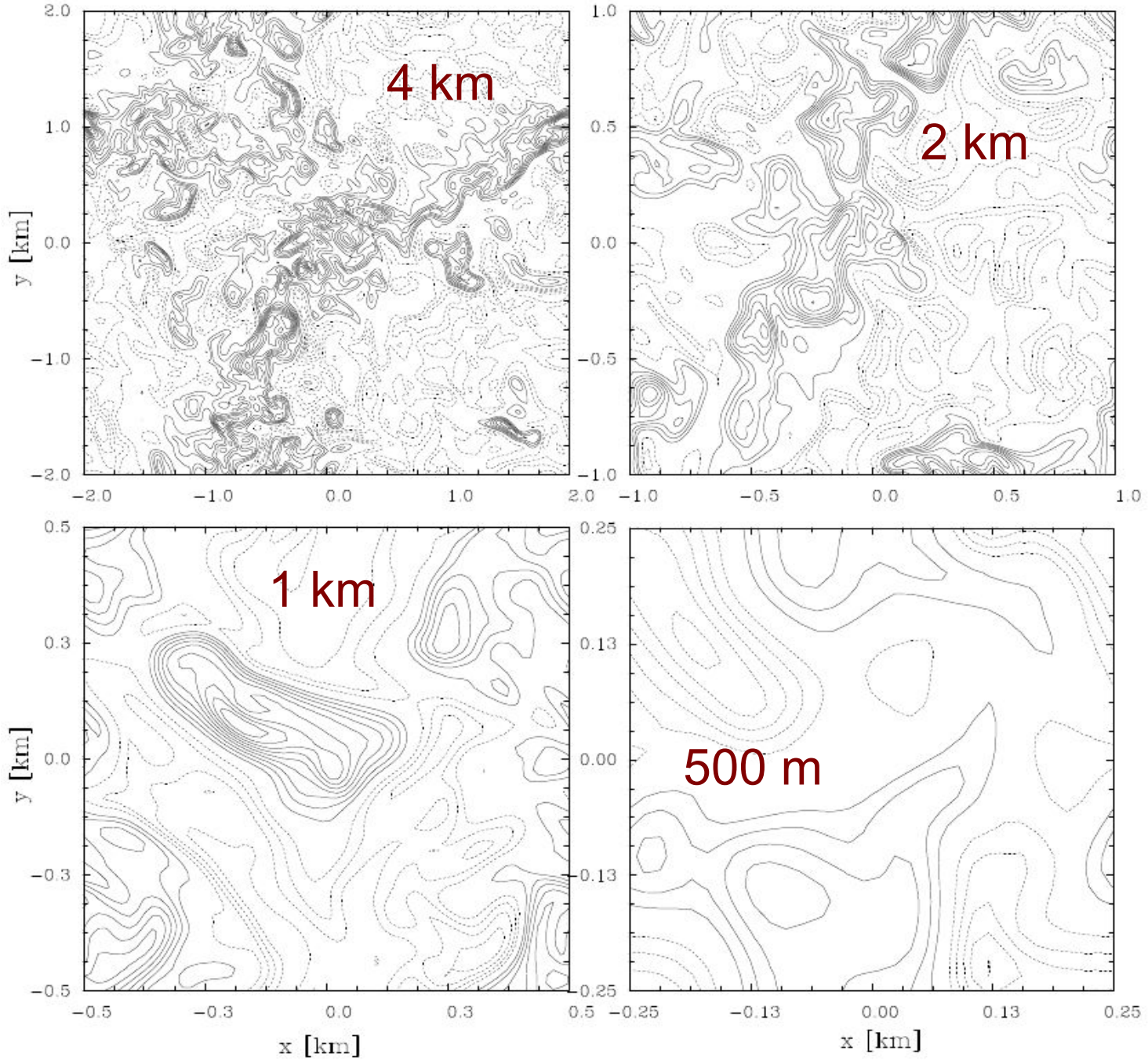

FIGURE 4.3.2. Vertical velocity as in Fig. 4.3.1 but for fixed $\Delta_H = 15$ m and variable horizontal domain.

Coarse-graining of high resolution simulation

DIFFERENT FROM LOW RES!!!

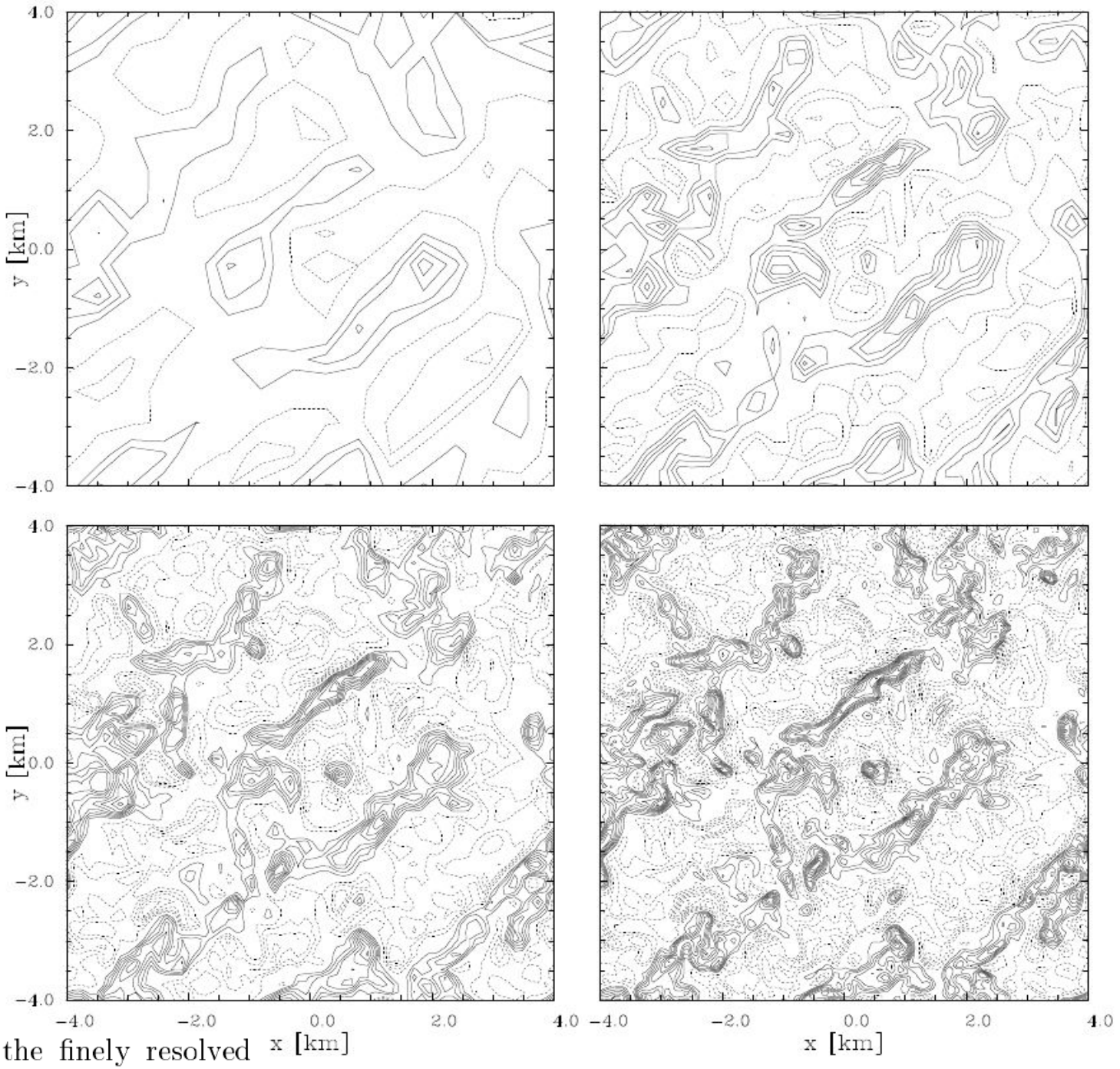

FIGURE 4.3.3. Vertical velocity of the finely resolved case in Fig. 4.3.1 (256^2 grid points in the horizontal) coarsened to horizontal resolutions of 128^2 (lower right), 64^2 (lower left), 32^2 (upper right), and 16^2 (upper left) grid points.

Result
- resolution and convergence requirements in the investigated case of typical atmospheric boundary layer:

at least 8km x 8km in horizontal to resolve 3 wavelengths;

maximum 60 m horizontal resolution to capture the convective roll size perpendicular to the mean wind.

- By product: spacing of rolls agrees with the prediction from linear theory.

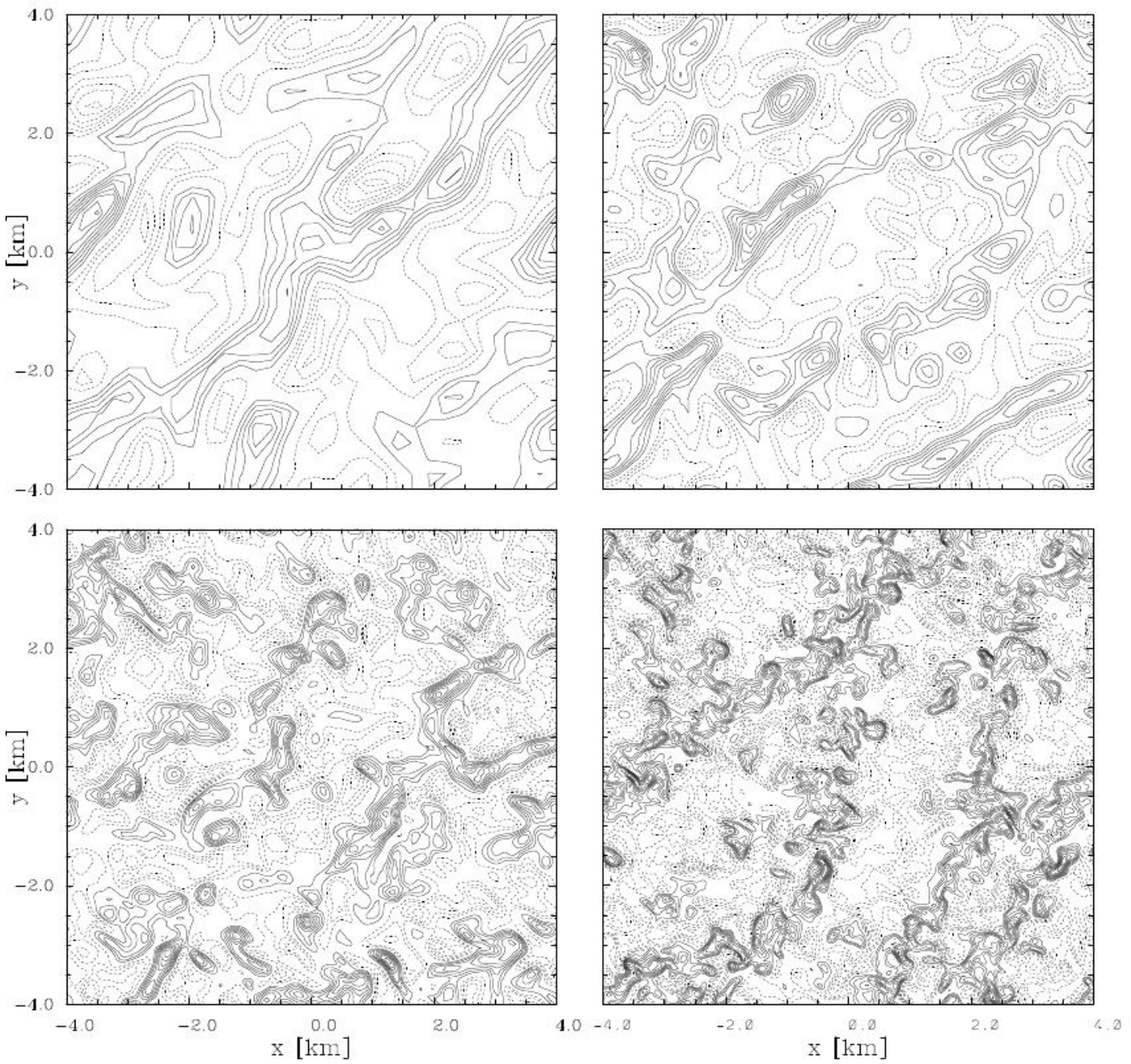

FIGURE 5.1.4. Vertical velocity as in Fig. 4.3.1 but for ILES.

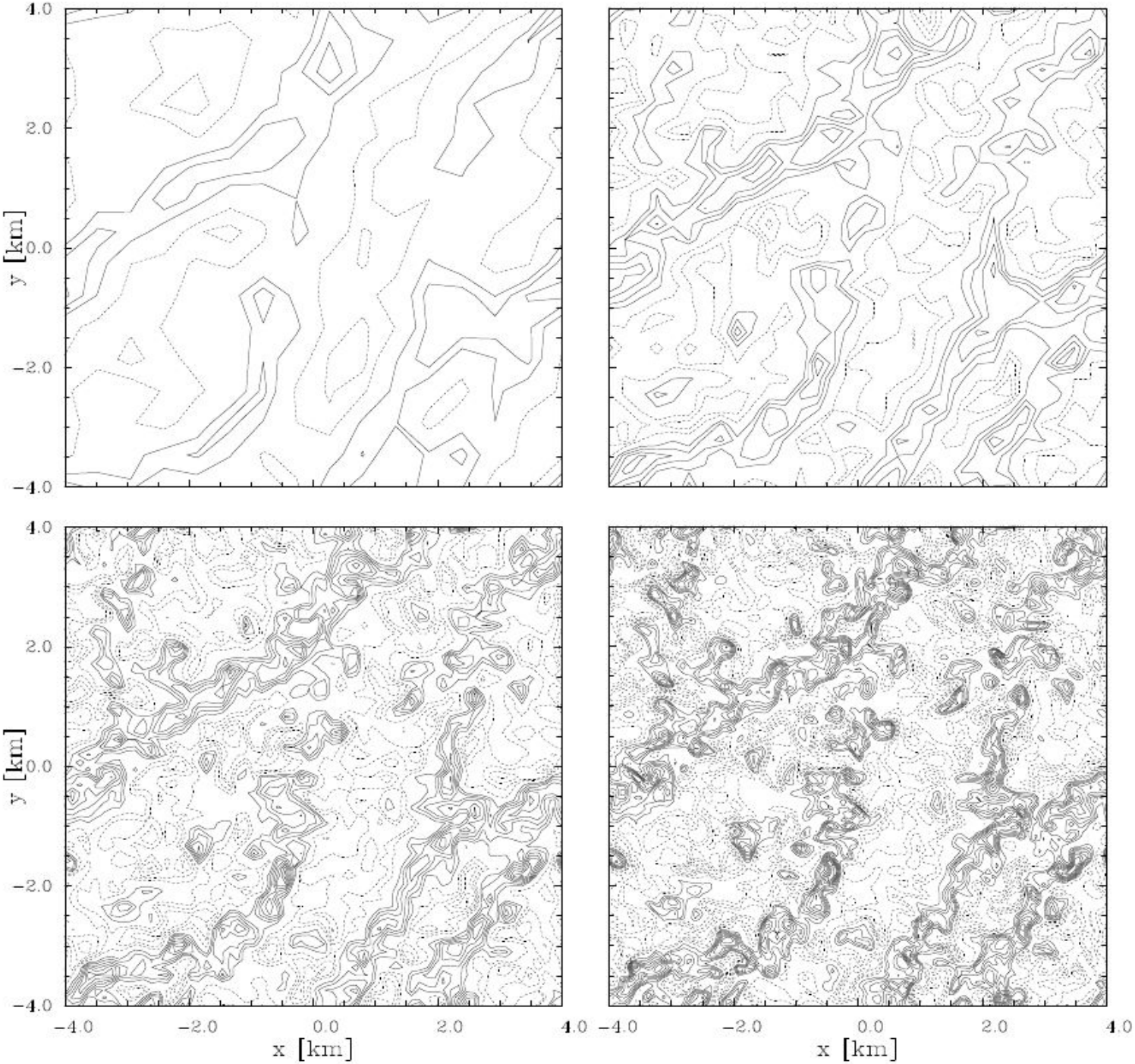

FIGURE 5.1.5. Coarsened vertical velocity of the finely resolved case, as in Fig. 4.3.3 but for ILES.

LES

ILES

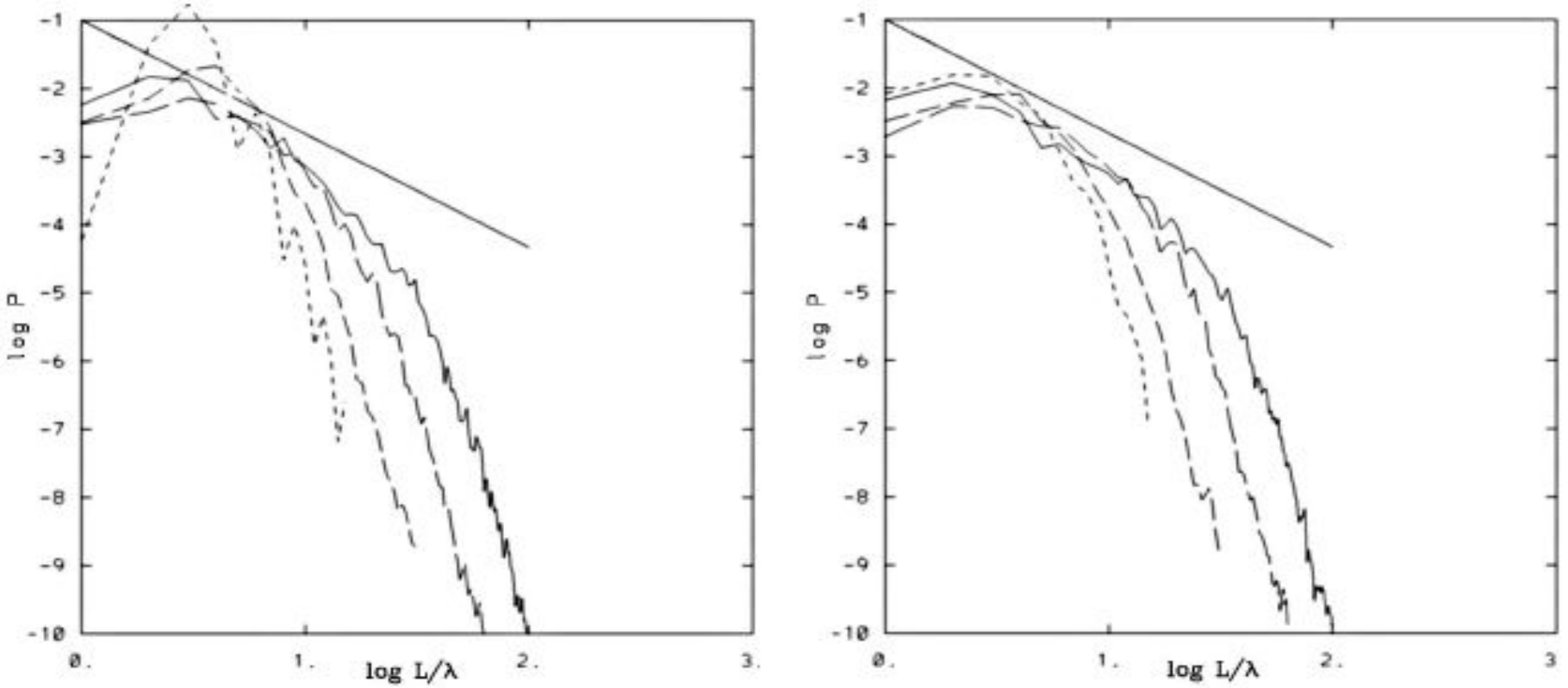

FIGURE 5.1.6. Diagonal ($k_x = k_y$) of the 2D power spectra P of vertical velocity at different Δ_H; left and right panels correspond to Figs. 4.3.1 and 5.1.4, respectively. The "-5/3" slope is shown for reference.

Various numerical realizations of anisotropic viscosity

- similar results!!!

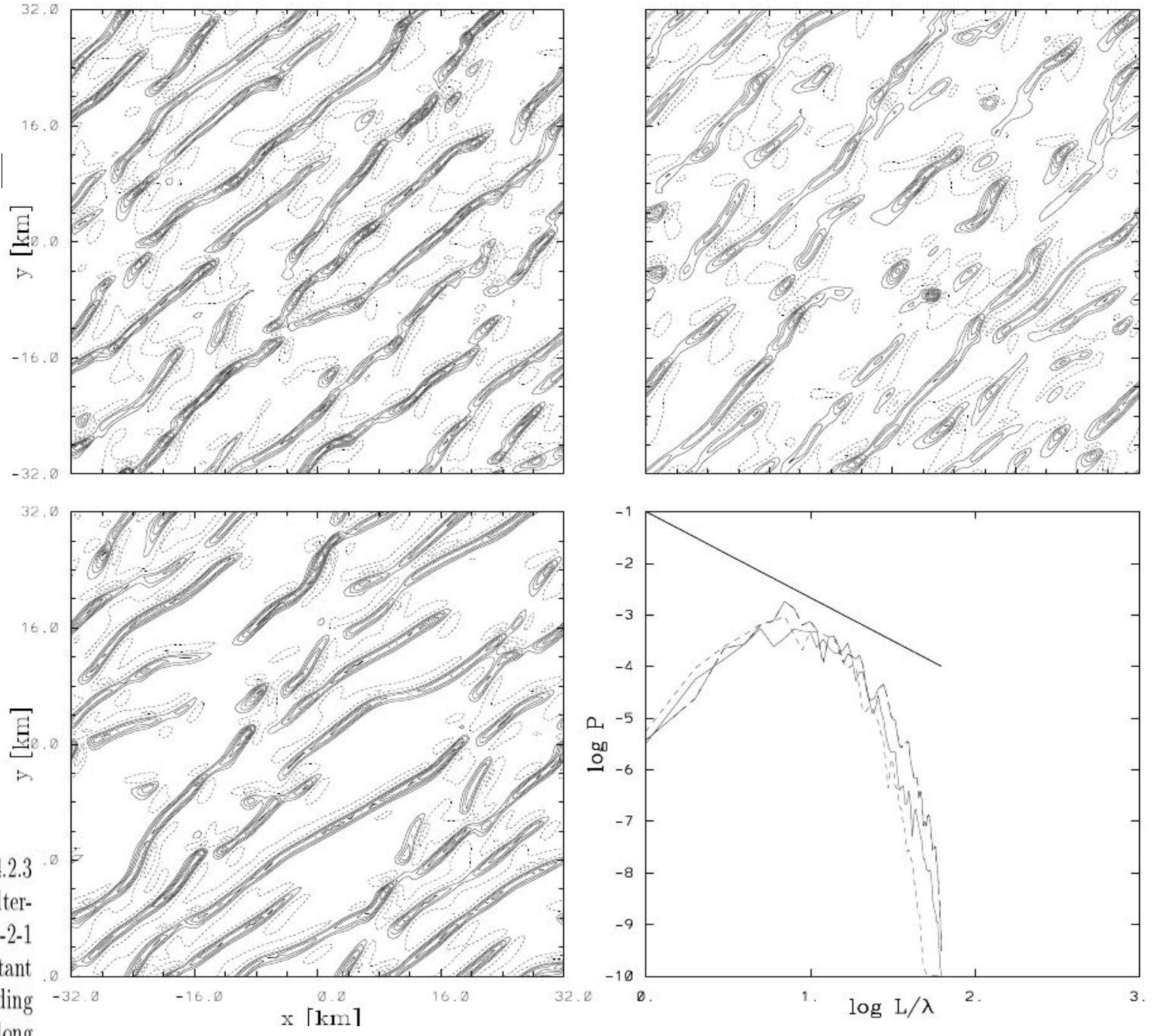

FIGURE 5.2.1. Vertical velocity at 450 m as in Figs. 4.2.3 and 5.1.3, but for runs with various anisotropic filtering: composite schemes (upper left); a periodical 1-2-1 low-pass filter in the horizontal (upper right); constant anisotropic viscosity (lower left); and the corresponding diagonals of 2D spectra (lower right) shown with long dashes, short dashes and continuous line.

CONCLUSION

The main stream of research in geophysical and astrophysical convection falls in the regime of large Rayleigh numbers. Rapid progress in computational technology already enables large- and global-scale simulations of convective fields at unprecedented meso-scale resolutions. This enables calculations free of convection parameterizations (viz. phenomenological models), in the spirit of LES.

Ironically, the simulated (as opposed to parameterized) convection can be largely under-resolved, making numerical solutions sensitive to ad hoc filtering present in some form in all computational models.

The latter shifts the virtual reality of convection toward moderate and low Rayleigh number regimes, rich in intriguing and attractive forms of the structural organization, yet unrealistic for the specified external parameter range.

Construction of convective experiments HOWTO

- Use best possible numerics to ensure that there is no spurious dissipation.
- Understand your model construction. Avoid implicit dissipation numerical methods, ad-hoc filters or subgrid-scale turbulence models that introduce excessive diffusivity.
- Be cautios about convective structures while performing mesoscale cloud resolving simulations.
- Carefully select numerical methods to simulate cloud resolving convection (e.g. MPDATA).
- Be very cautious when analyzing convective cloud shapes, sizes or cloud coverage.
- Reference:
- Piotrowski Z.P., Smolarkiewicz P.K., Malinowski S.P. and Wyszogrodzki A.A.: On numerical realizability of thermal convection, J. Comput. Phys. (2009) doi:10.1016/j.jcp.2009.05.023

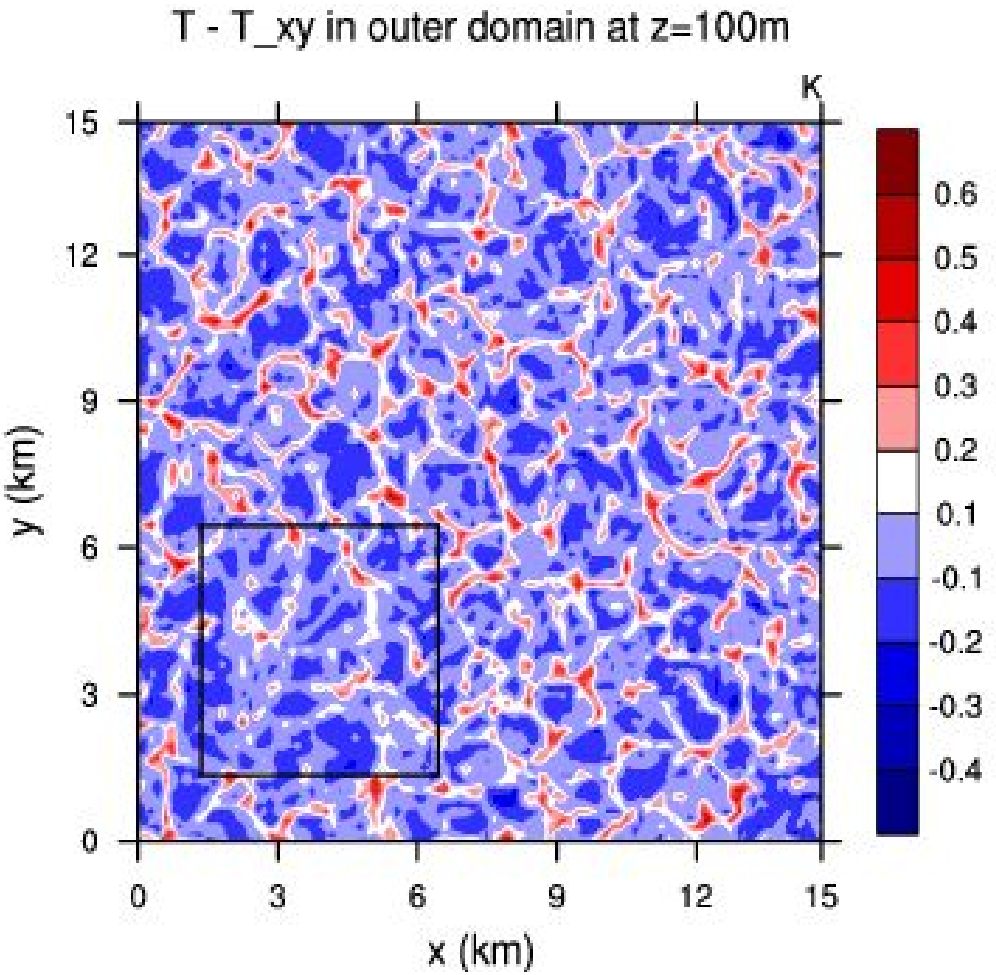

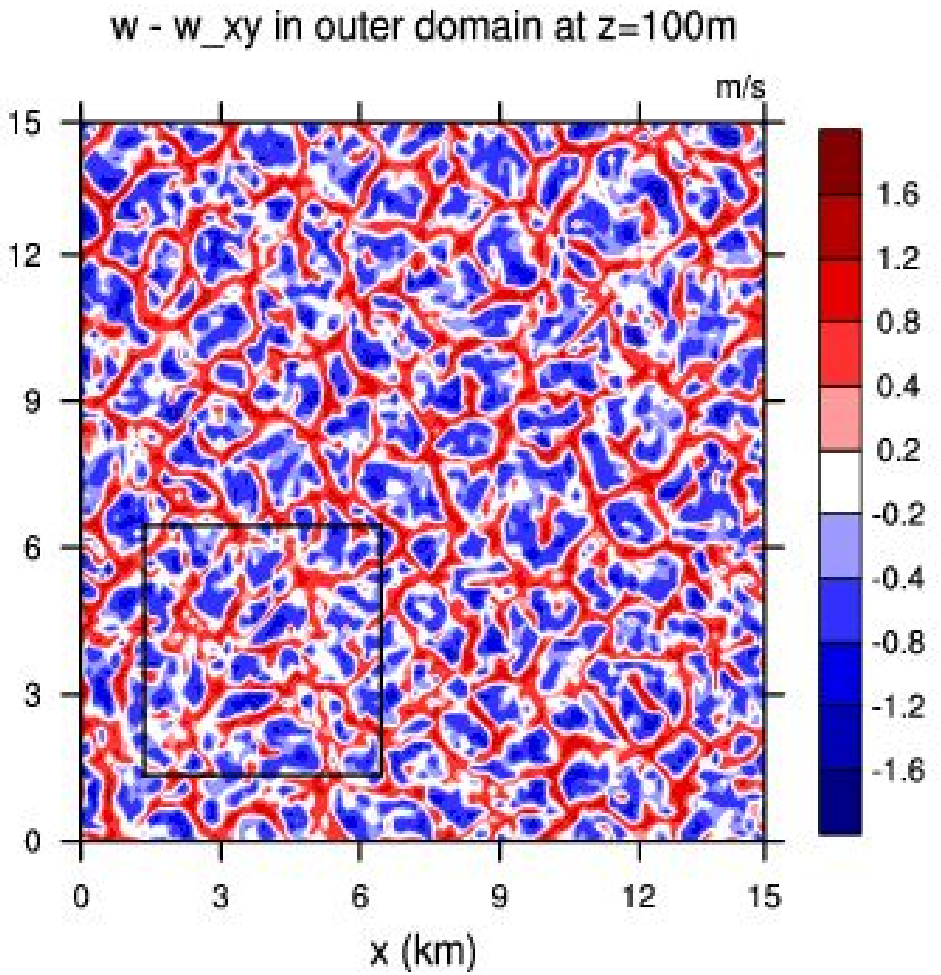

http://www.essl.ucar.edu/LAR/2006/strategic-goals/sp5/sp5.htm

The two simulated turbulent flows (see figure) blend in smoothly across the nesting boundaries, and produce similar statistics, which also compare well with previous LESs. Future plans for ESSL/MMM scientists include expanding this nest-LES study for more complex and realistic PBLs, such as those with clouds, over realistic surface conditions, and interacting with mesoscale events and deep convection.

TRUE or FALSE???

Characteristics of Mesoscale Organization in WRF Simulations of Convection during TWP-ICE

ANTHONY D. DEL GENIO

NASA Goddard Institute for Space Studies, New York, New York

JINGBO WU AND YONGHUA CHEN

Department of Applied Physics and Applied Mathematics, Columbia University, New York, New York

(Manuscript received 6 August 2011, in final form 4 February 2012)

The simulation domain is 280 km x 280 km, centered on Darwin at 600-m resolution with 50 vertical layers and realistic geography [Bryan et al. (2003) recommend a resolution of ~100 m for deep convection, but Del Genio and Wu (2010) and Romps and Kuang (2010) find that the coarser resolution produces similar results except for slightly weaker entrainment and mass flux].

TRUE or FALSE???

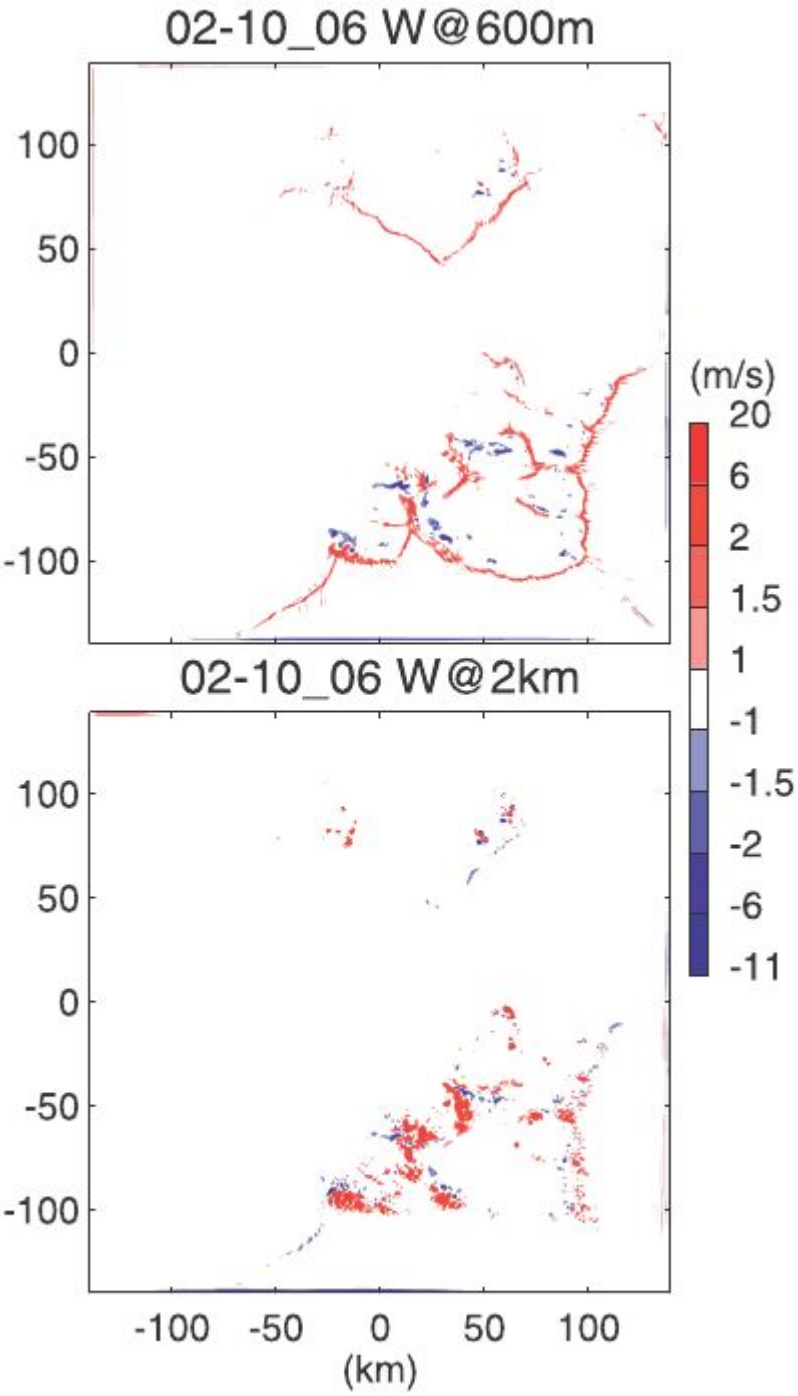

3. 9. Simulated 10-min average vertical velocity field at (top) 600 m and (bottom) 2-km altitude at 0600 10 Feb 2006.

- But...

Resolution and domain-size sensitivity in implicit large-eddy simulation of the stratocumulus-topped boundary layer

Jesper G. Pedersen[1], Szymon P. Malinowski[1] and Wojciech W. Grabowski[2]

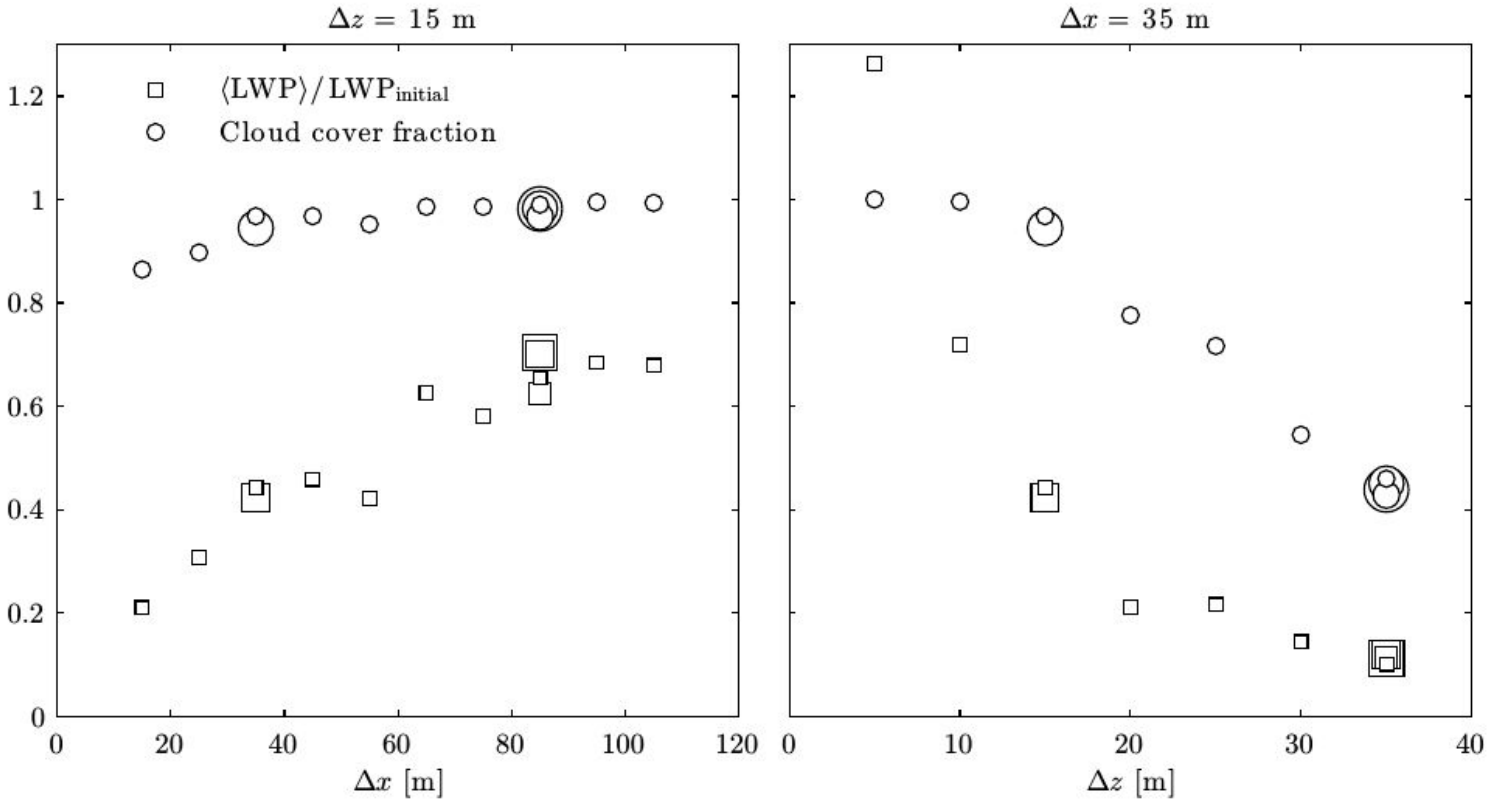

Figure 1. Domain-averaged LWP relative to the initial value $\mathrm{LWP}_{\mathrm{initial}}$ (squares) and cloud cover fraction (circles) as functions of Δx in the left panel and of Δz in the right panel. Both quantities are averaged over the period between 240 and 360 minutes of simulation time. The symbol size increases with domain size.

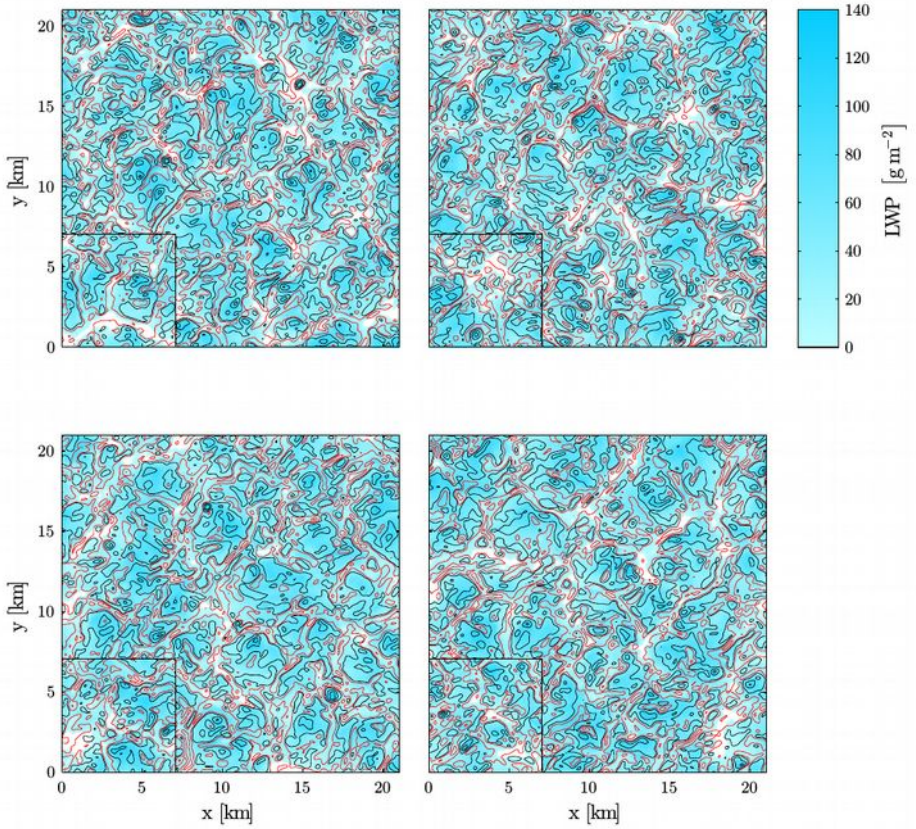

Figure S3. Updrafts, downdrafts, and LWP from simulations $D_{85,15}$ and $B_{85,15}$ after 240, 280, 320, and 360 minutes (left to right, top to bottom). The cross sections from the small domain ($B_{85,15}$) are inserted in the lower left corner of the cross sections from the big domain ($D_{85,15}$).

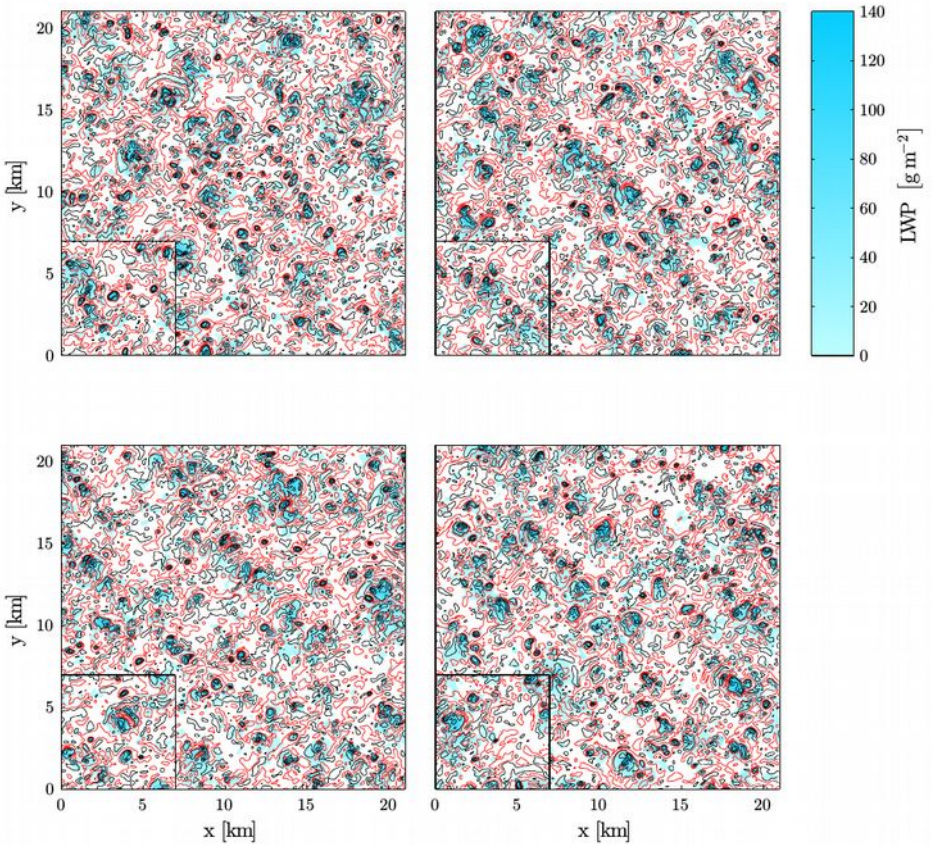

Figure S4. Updrafts, downdrafts, and LWP from simulations $D_{35,35}$ and $B_{35,35}$ after 240, 280 320, and 360 minutes (left to right, top to bottom). The cross sections from the small domai ($B_{35,35}$) are inserted in the lower left corner of the cross sections from the big domain ($D_{35,35}$).